

# Experiments on scan shifts correction for coherence scanning interferometry

HUSNENI MUKHTAR<sup>1</sup>, PAUL MONTGOMERY<sup>2</sup>, FREDDY ANSTOTZ<sup>2</sup>, RÉMI BARILLON<sup>3</sup>,  
KUSNAHADI SUSANTO<sup>4,5</sup>, WILLY ANUGRAH CAHYADI<sup>1,\*</sup>

<sup>1</sup>*School of Electrical Engineering, Telkom University, Jl Telekomunikasi no.1, Bandung, 40257, Indonesia*

<sup>2</sup>*ICube Laboratory, University of Strasbourg-CNRS, 23 rue du Loess, Strasbourg, 67037, France*

<sup>3</sup>*IPHC, University of Strasbourg-CNRS, 23 rue du Loess, Strasbourg, 67037, France*

<sup>4</sup>*Geophysics, Universitas Padjadjaran, Jl Raya Jatinangor km 21, Jatinangor, 45363, Indonesia*

<sup>5</sup>*Institut de Physique du Globe de Strasbourg, University of Strasbourg-CNRS, 5 rue René Descartes, 67084 Strasbourg, France*

---

In this paper, a solution is proposed for solving the lateral shift of the scanned images stack in coherence scanning interferometry (CSI). Pre-image processing is performed on a captured stack of scanned images of square structures without the fringes. It is useful to identify the lateral shift response, which is then utilized to correct a subsequent series of scanned images with fringes having the same optical scanning parameters. Thus, eliminating the scan-line shift in the reconstructed images. The experiments results show that the error due to the scan-line shift can be improved qualitatively and quantitatively by around 0.6 - 0.7% at the lateral axis.

(Received May 16, 2023; accepted October 6, 2023)

Keywords: Scan shift, Misalignment, Vertical scanning, Coherence scanning interferometry, Image processing

---

## 1. Introduction

Coherence Scanning Interferometry (CSI) has proven itself to be one of the profiler methods in measuring surface roughness of microscopic objects. Both qualitative and quantitative studies of different materials based on CSI images are offered from the imaging result. Examples of quantitative ones of surface roughness and morphology may be found in the fields of metrology, advanced materials, and surface inspection in the industry [1-6]. Despite the presence of commercial interferometers such as Mahr, Polytec, Taylor Hobson, Veeco, Fogale and Zygo, many researchers have built and developed profilers to develop enhanced methods and improved results [7-11] using different interference objectives such as Mirau and Linnik. For example, a modified Linnik Fogale interference microscope developed in the ICube laboratory IPP is able to work in liquid medium [12] having a lateral resolution of around 0.55  $\mu\text{m}$  with 20x magnification lens and a vertical error of 1.6% from vertical calibration using a step height artifact.

A good imaging result of the surface structure of microscopic objects in 3 dimensions (3D), generated by two-dimension image stack from lateral scanning with optical profilers such as CSI and optical coherence tomography (OCT), has become a priority requirement in obtaining information and facilitating the analysis process. However, either poor or inaccurate results in scanning profilers can be produced due to several factors. Exploring the causative factors in OCT, we found similar problems in some studies, i.e., there were thickness measurement

errors in stratus OCT [13] where the retinal nerve fibre layer was strongly affected by signal strength and horizontal scan shifts, while the vertical shifts can be neglected. These shifts were caused by improper alignment during scanning. To avoid the misalignment, another OCT scan study demonstrated either the calibration step for obtaining more precise results and the accuracy improvement with stable room temperature and limited number of scans [14] while to correct the artifacts or shifted image in simultaneous scanning OCT, comparison of the position data between the misaligned and reference OCT scans of retinal layer thickness image was well performed [15]. According to an invention [16], the effect of misalignment between pixel images generated by an array of modulator elements can be ameliorated by using an optical system with a single modulator array to overlap the separate rows.

Like in any other measurement technique, CSI also has sources of errors and uncertainties in the measurements, which can be classified into two broad categories [17]. The first category comes from the uncertainties in the vacuum wavelength and in the refractive index (arising from the absence of correction or the input used for the correction) and the cosine error. The second category includes the uncertainty in the phase change measurement, cyclic errors, dead path effect, Abbe error, target error, optics thermal drift, beam shear, data age uncertainty, and the effects of fringe scanning. Concerning the last point, any lateral motion between the scanning stage and the camera target can constitute a source of measurement uncertainty, especially for surfaces

with steps of texture. For decades, some problems concerning the studies of CSI development were reported in many publications such as decreased contrast and asymmetrical interferogram plot due to misaligned beam splitter (in Mirau and Taylor), the chromatic mismatch and glass dispersion (in Linnik) [18], misaligned data due to the drift [19], the batwing effect in white light interferometry due to the shorter step height than the light source coherence length [20], lateral error due to dispersion effect in Mirau type and conical illumination [21], and other uncertainty error sources due to installation, optics, electronics, environmental effect, motion error, and dead path [22-26]. Further, due either to a non-linearity in the motorized-piezoelectric translation actuator [27] or a misalignment of the microscope construction [28], the series of scanned images during scan process may exhibit a lateral shift over successive images, which can lead to measure artifacts. In addition, any lateral movement of the sample during fringe scanning, whether the sample is mounted on a vertical scanner, or the interferometer head itself, leads to artifacts in the surface measurements. In consequence the stability of the measured object during scanning is therefore important for measurement precision [29, 30]. Those problems may be

overcome by improving the optical component quality, adding the built-in correction system of hardware or software [31], instead a high-resolution interferometry may decrease.

Considering a study of artifacts due to the scan-line shift on another type of microscopes, namely scanning electron microscope, Maragechi et al. [32] conducted a comprehensive method to correct the shift artifacts using a novel global DIC framework. They reported that the significant errors of geometrical measurement in full field deformation by digital image correlation (DIC) were caused by the electron beam position error during scanning [33, 34]. For the CSI case, a detailed account of what are the scan-line shift artifacts is illustrated in Fig. 1. A CSI image of etched Silicone with dimensions of  $132 \times 127 \mu\text{m}$  is presented on the left side. On the right, two consecutive scan images of a zoomed view of the same image are compared vertically and horizontally. The first scan image,  $i_1$ , compared to the 279<sup>th</sup> scan image, has line shift in horizontal, but not in vertical. The shift is marked by the indicators showing a part of the feature in the first scan image moving to the right in the 279<sup>th</sup> scan image.

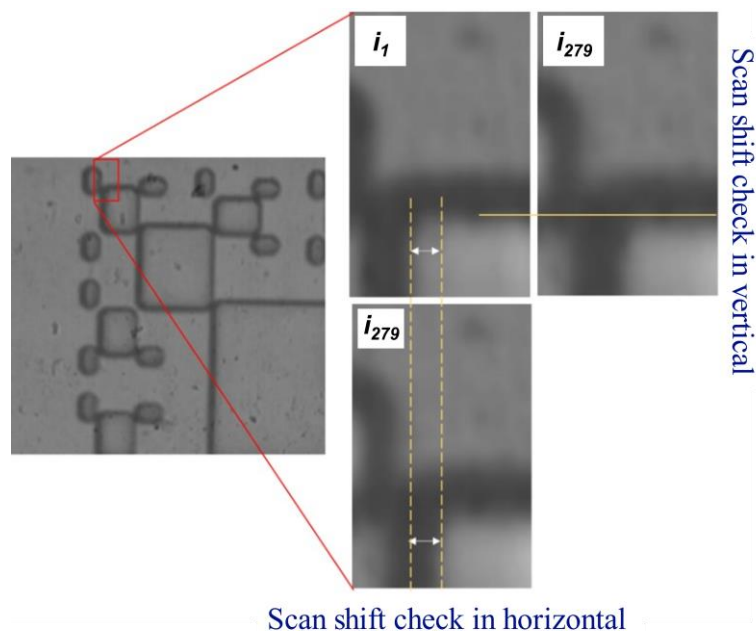


Fig. 1. The illustration of scan-line shift image during scanning (color online)

This finding then raises a question. Some possible causes of this shift could stem from the aspects of stability, alignment, calibration, etc. However, for a modified Linnik Fogale microscope developed at the ICube laboratory, these reasons cannot be the main cause since the microscope has been calibrated beforehand. Moreover, the microscope was validated with other commercial microscopes and the measurement result was similar to them [12]. Profiles from the 3D measurement results showed a slope on the step features perpendicular to the x-axis, but not on those perpendicular to the y-axis, showing

that the accuracy of the measured results were affected by the lateral image movement during vertical scanning. For some reason the scanner was misaligned along the x-axis.

However, it was difficult to determine whether the misalignment was of a mechanical or optical origin to implement a correction. Moreover, there was an uncertainty concerning how much shifting occurred and at what point during the scanning. Therefore, as an alternative solution, a method is proposed to simply measure the image shift during scanning and to correct the image positions of the scanned images in one direction

before performing fringe processing. In the following, the experimental system is first described together with the test sample used. Then the method developed for image correction is explained and applied to image acquisition. Finally, the corrected measurements are compared with those without the correction to demonstrate the validity of the technique.

## 2. Experimental methods

This section elaborates the shifting correction of CSI image stacking acquisition. The suspected shifting images occurred on a few micrometres and either in single or double direction ( $x$  or  $y$  direction). To provide a high-quality CSI stacking image, the suspected shifted images

should be moved back to the original position. The number of shift images is detected by a simple algorithm that will be described in the experiment setup.

### 2.1. Experimental setup

In the data acquisition of the CSI technique, along the dynamic range (DR), the piezoelectric stepper does the vertical scanning movement for each step-height ( $dz$ ), then a series of scanned images were obtained. The values of DR and  $dz$  are determined prior to the acquisition process. A stack of scanned images is processed from the grayscale image (heights) and the maximum intensity image using the five-sample adaptive (FSA) fringe visibility algorithm [8].

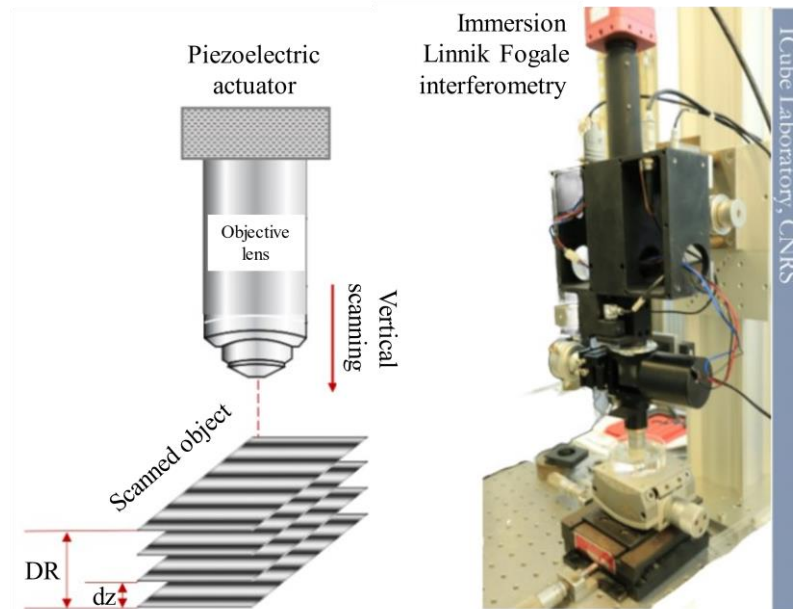


Fig. 2. A vertical coherence scanning interferometry moved by a piezoelectric actuator moves by steps of  $dz$  over a dynamic range of  $DR$  (left). Mechanical diagram of modified Fogale Linnik system (right) (color online)

In this experiment, the microscope is mounted on a robust aluminium column installed onto the optical table to provide good stability to the whole system. A microscope focusing mechanism provides vertical movement adjustment of the microscope, with fine and normal

focusing. Two mounting plates (illustrated in Fig. 2) are used to mount the microscope body and the position adjustment to the column. However, the vertical scanning still yields the misaligned stacking images due to the unstable motorization system.

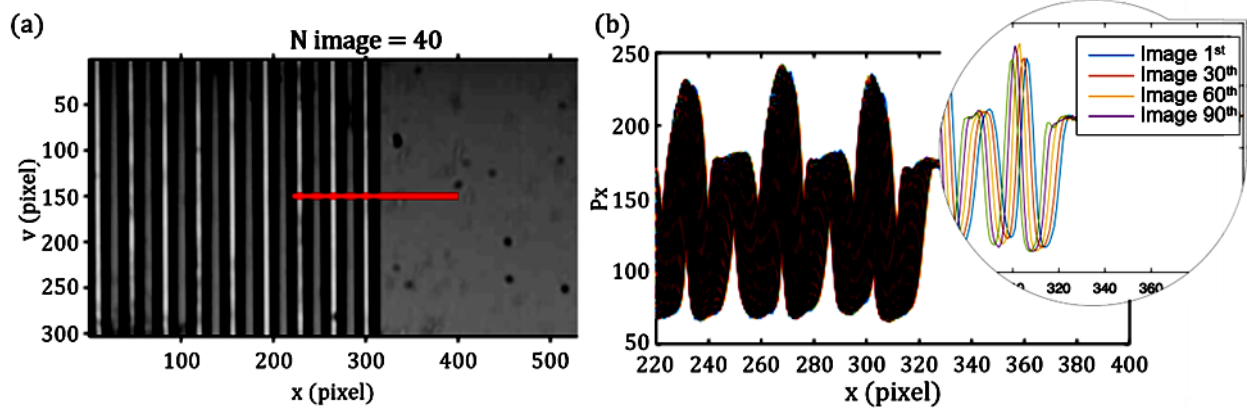


Fig. 3. The lateral image shifting during the axial scanning over  $5\mu\text{m}$ -DR using the  $20\times$  immersion Linnik: (a) displacement test of a sample on the measured area for the displacement test, (b) Line profile from a scanned image stack (a zoomed view in specific area) (color online)

## 2.2. Data test acquisition

As previously mentioned, lateral shifts in one direction could be observed by eye in the images during the vertical scanning process. A specific sample was required to be used with the grating positioned perpendicular to confirm and quantify this shift. Thus, an etched grating sample was used with the grating positioned perpendicular to the shift direction. A series of images of an etched grating sample were captured while scanning over a depth of  $5\mu\text{m}$  (shown in Fig. 3). A lateral shift of the measured sample during the scanning process can be observed on a series of successive images. These shifts were most likely caused by a microscope misalignment along one direction in the vertical scanning perpendicularly.

In this experiment, we scanned a grating object as consecutive images. A total of 91 consecutive images were scanned using CSI Linnik immersion equipment to prove that the scan line was misaligned. If the misalignment is ignored in the consecutive images, it will lead to artifact generation and ruin the surface profile calculation.

The correction method starts with a procedure of acquiring the test data carried out in two stages: first, acquiring a set of the test data; second, the implementation of the correction method. Correcting the image shifts was begun by vertically scanning the object surface without any fringes to acquire a stack of scanned images that could be used to obtain the shift parameters. Once the corrected fringe images were obtained, they could be used in the next subsequent image processing employed in the CSI technique.

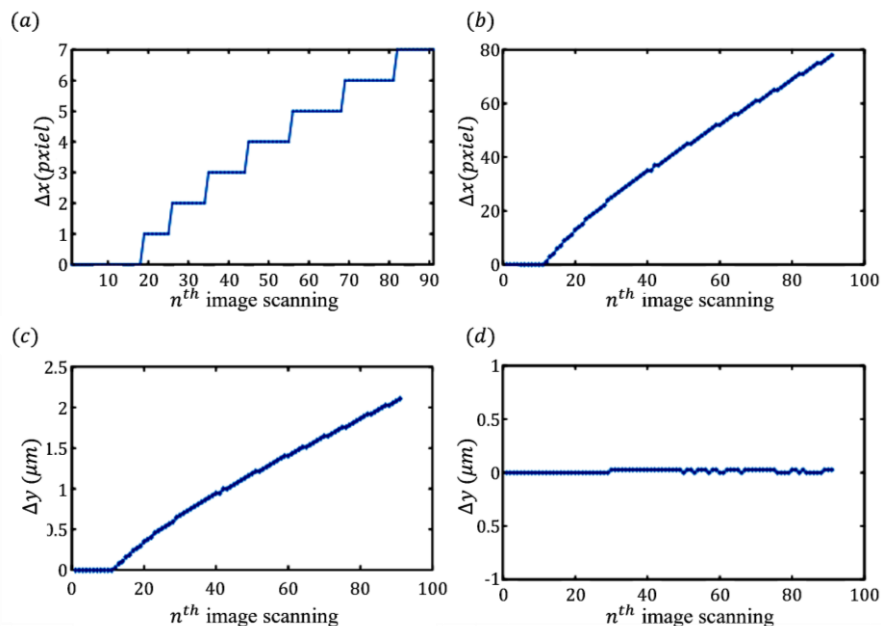


Fig. 4. The successive images with  $5\mu\text{m}$  of the dynamic range,  $\lambda_{\text{eff}} = 450\text{ nm}$ ,  $dz = 0.056\mu\text{m}$  and the  $20\times$  immersion objective. The results of the cross-correlation function for (a) the lateral shift in x-axis (pixels) between sequent images, (b) The shift in x-axis between two images after executing  $10\times$ -pixel-resampling using an interpolation of a cubic kernel in pixel unit and in (c) micrometre unit (d) the shift in y-axis ( $\mu\text{m}$ ) (color online)

### 2.3. Correction method

A simple correction method for the image shift was applied to improve the image scanning.

The method was carried out using the following procedures.

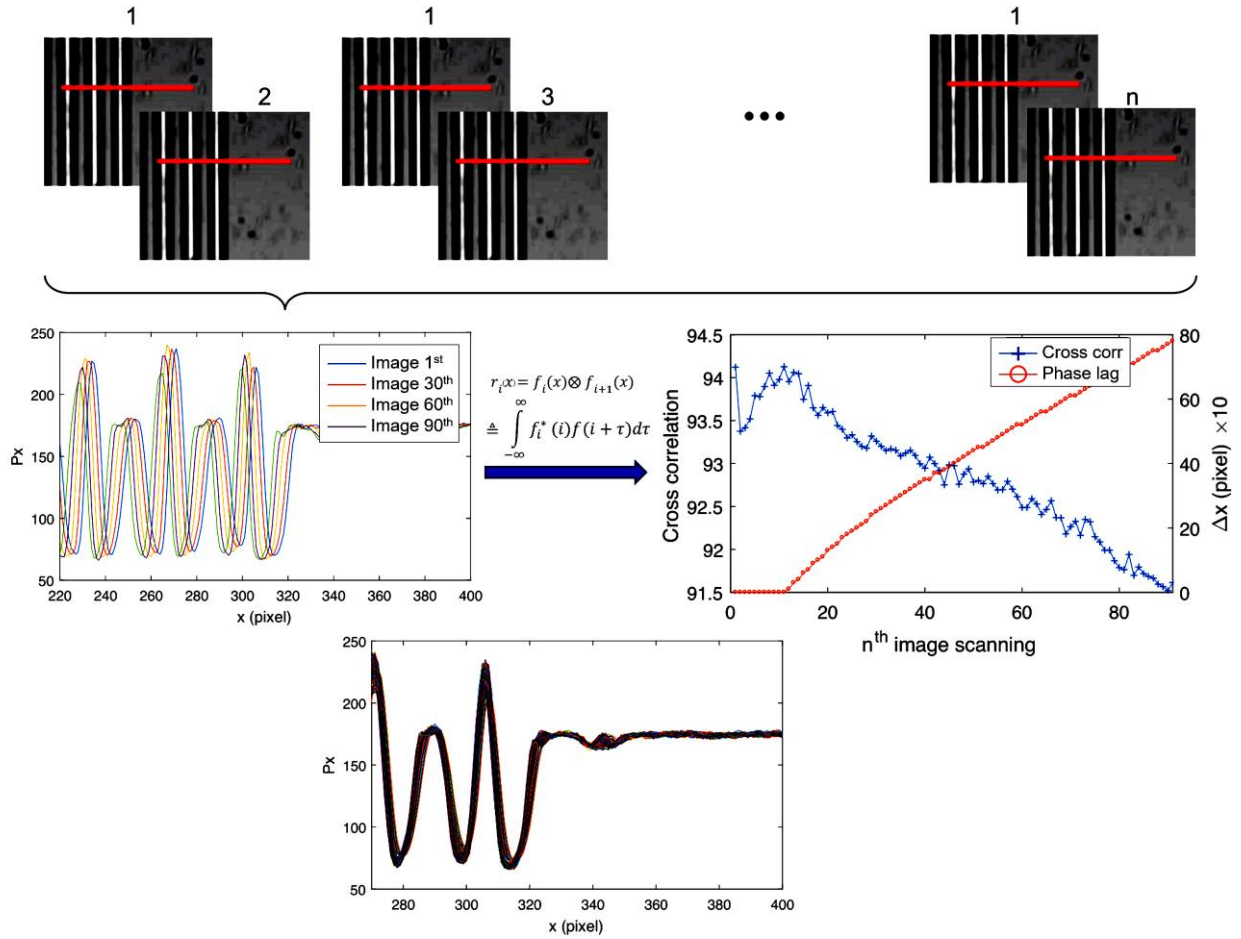


Fig. 5. A result examination of the proposed method using cross correlation. The shifted images are defined by the phase lag of sine grating response. The images were resulted from  $20\times$  magnification lens,  $10\ \mu\text{m}$  dynamic range and  $0.056\ \mu\text{m}$  step height (color online)

1. Examining the displacements over the images. The spatial correlation method was used for different step height ( $dz$ ), DR, and lens magnification in order to acquire the displacement function. Fig. 4 shows the technique. The correlation function for estimating the shifted image is expressed in Eq. 1.

$$r_i(x) = f_i(x) \otimes f_{i+1}(x) \triangleq \int_{-\infty}^{\infty} f_i^*(i) f(i + \tau) d\tau \quad (1)$$

where  $r$  is the spatial lag between two scanned images,  $x$  is a pixel representing spatial image in  $\mu\text{m}$  unit,  $i$  is the index image,  $f_i$  is the reference image,  $f_{i+1}$  is the examined images, and  $\tau$  is the phase due to misalignment. The image shifting, using this technique, could only be discovered by 1 pixel-units of the shifts over the whole images, yielding displacement about 0.15 – 0.2 pixels/ image.

Hence, one could not find the shift from image 1 to 18 in Fig. 4(a) because of the inability to detect the pixel fractions. Detection of the image shift is therefore necessary to improve by utilizing a resizing technique.

2. Resampling the image to update the detection of shifting. The size and the number of the image increases by enhancing the image by pixel resampling as shown in Fig. 4(b). This technique used cubic kernel interpolation to find the shift in the upscaled images.

3. Based on the second procedure, all sets of resized images are corrected using Eq. (1) in reverse direction so that the details on the images would be in their correct positions. It was assumed that the correction procedure was spatially periodic, written in the following expression: *shifted* = *circshift*(*image*, [1 -  $r$ ]).

4. Restoring the resized images to original size (second resizing). The original image compared with the corrected can be seen in Fig. 5.

A complete proposed method for the image scan correction due to the scan-line shift is summarized in Fig. 5. Successive profiles of the grating (Fig. 5, top left) before correction of the image shift measured in the same area using the Eq. 1, and (Fig. 5 bottom) after correction of the image shift.

The investigation result of the data yields an important observation. It confirmed that the correcting image was required only in one direction ( $x$ -axis) because there was no significant lateral image shift along the  $y$ -axis as seen

in Fig. 4 (d). The mean values of the displacement between two consecutive images using Eq. (2) were around  $0.025 \mu\text{m}$  and the total displacement for a full scan was  $1.587 \mu\text{m}$  or approximately 5-6 pixels. The total lateral shift was less than  $0.18 \mu\text{m}$ , and thus could be ignored.

$$\Delta\bar{x} = \frac{\Delta x_n - \Delta x_{n-1}}{n-1} \quad (2)$$

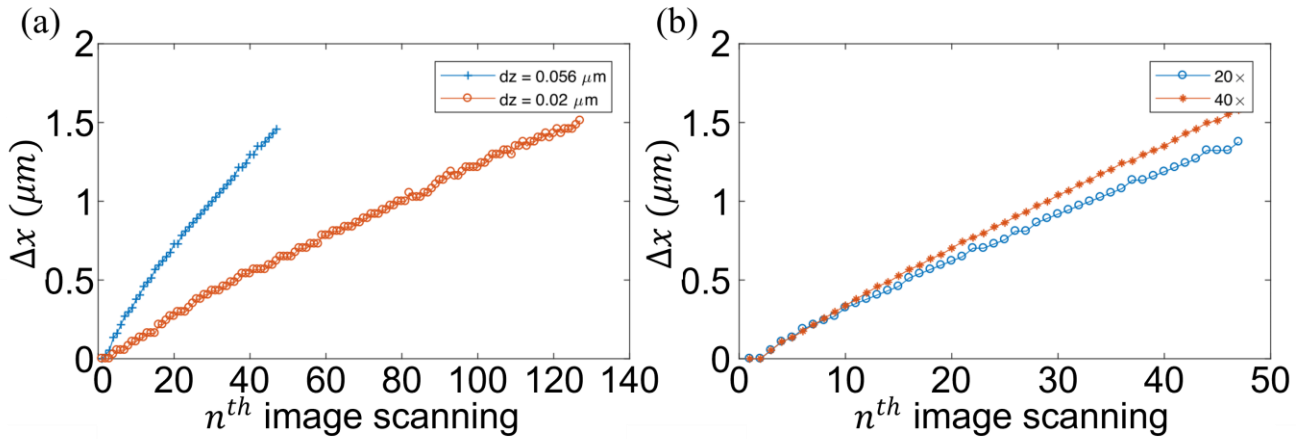


Fig. 6. The scan-line shift with differences of (a) step height and (b) lens magnification (color online)

Upon further investigation, the scan-line shift by differences of the step height and the lens magnification over the same dynamic range was presented in Fig. 6. The shift total for both step height is similar, i.e., approximately  $1.5 \mu\text{m}$ . It means that the total shift will depend on the dynamic range or the distance of the scanning process. On the contrary, the scan-line shift due to the different lens magnification is not that different.

In this section, the developed correction method provides a software solution for correcting the axial misalignment of the microscope leading to a shift in the acquired fringe images during vertical scanning in the CSI technique, as illustrated in Fig. 5.

### 3. Results and discussions

The correction method was then tested on a series of fringe images acquired for measuring some samples etched in a silicon wafer, as previously mentioned [12]. Samples were measured by Fogale Linnik water immersion system ( $20\times$  magnification,  $\text{NA}=0.5$ ,  $dz=0.056 \mu\text{m}$ ,  $DR=5\mu\text{m}$ ,  $\lambda_{\text{eff}}=450 \text{ nm}$ ) with white light LED. After

processing the scanned images of grating sample using the FSA algorithm without treatment of proposed correction method (Fig. 7 (a) and (b)), it can be observed qualitatively that the walls between the holes (dark areas) are widened, and the valley bottoms are over-rounded. On the contrary, the completely corrected scanned image (Fig. 7 (c)), shows narrower walls between the etched holes and the squarer bottoms of the valleys.

In order to investigate not only the qualitative result but also the quantitative one for using the proposed method, then the grating pitches were measured as presented in Table 1. The mean length and height of pitch in respectively are  $10.00 \mu\text{m}$  and  $2.10 \mu\text{m}$  for the corrected scan image and  $9.94 \mu\text{m}$  and  $2.10 \mu\text{m}$  for the uncorrected scan image. This sample was also measured in previous research by a commercial microscope, namely Mirau Zygo New View 7200 with  $50\times$  magnification, resulting  $10.00 \mu\text{m}$  of mean length and  $2.06 \mu\text{m}$  of mean height 0. Both sizes were similar among them, having the same accurate length. The pitch length of uncorrected image was slightly different about 0.6% compared with the corrected image. This further reinforces the fact that the shift does occur in the  $x$ -axis and affects the measurement accuracy.

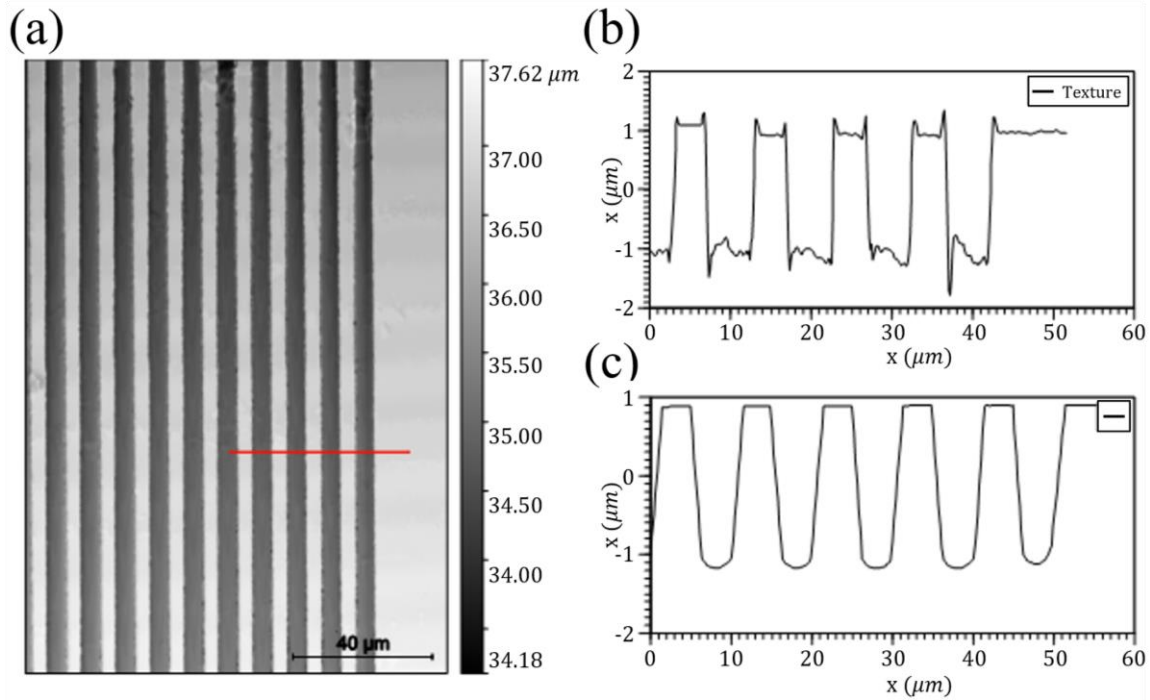


Fig. 7. Comparison of the measured profiles observed on (a) area of grating image indicated by line marking. (b) The uncorrected and (c) corrected images were demonstrated to show the benefit of the proposed method to correct the artifacts on the image (color online)

Table 1. Comparison of pitch size (in  $\mu\text{m}$ ) on an etched silicone (in Fig. 7)

No	Corrected		Uncorrected	
	Length	Height	Length	Height
1	10.00	2.10	10.00	2.12
2	10.00	2.10	10.00	2.10
3	9.88	2.10	9.76	2.10
4	10.12	2.10	10.00	2.13
Mean	10.00	2.10	9.94	2.10

Table 2. Comparison of pitch size (in  $\mu\text{m}$ ) on an etched silicone (in Fig. 8)

No	Corrected		Uncorrected	
	Length	Height	Length	Height
1	12.52	2.74	12.52	2.70
2	12.50	2.74	12.54	2.72
3	12.50	2.75	12.54	2.72
Mean	12.50	2.74	12.55	2.72

Taking the same procedure for another etched Silicon with valley texture, a line profile was examined, indicated by a horizontal line on the same area in Fig. 8. One can see that the uncorrected image scan shift has more artifacts than the corrected one. Meanwhile the pitch measurement, shown in Table 2, provided another fact of occurring the scan-line shift in x-axis denoting by 0.7% of the accuracy error of the length size. The same accurate length

compared to the previous result 0 offered a finding for the proposed method in this study. Another study with Atomic Probe Microscopy 0 also obtained minimal error using an offline algorithm of shifted or drift image using cross-correction based computer vision. It can be noted that the benefit of the proposed method in this study was improving both qualitative and quantitative results.

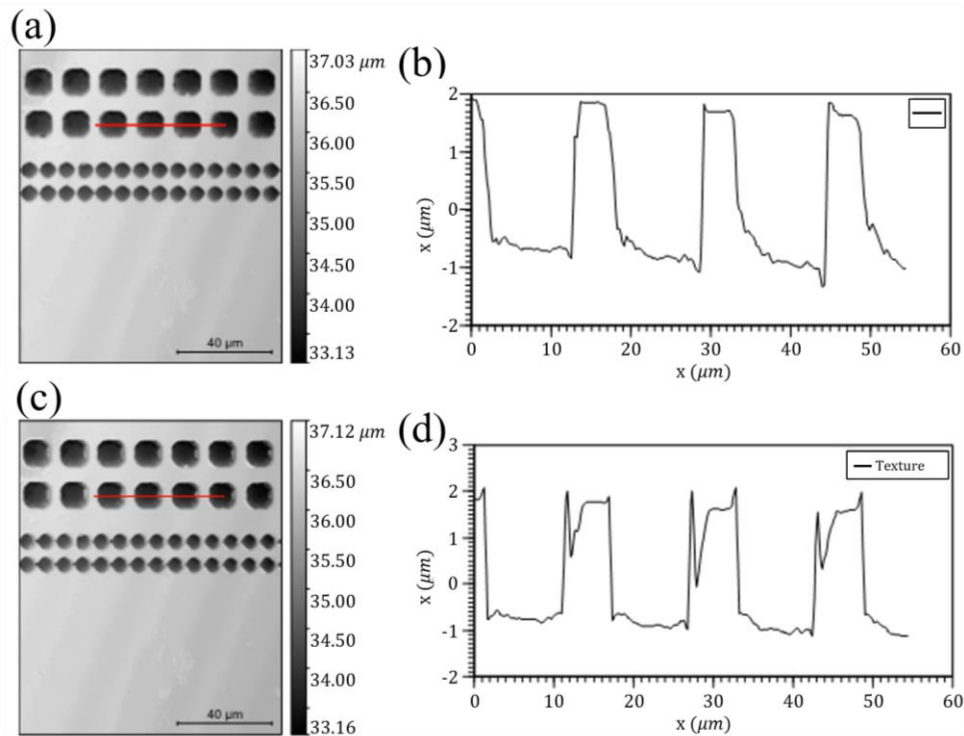


Fig. 8. Comparisons of resulting images (a)(c) and line profiles on etched silicon (b)(d). A line marking applied on same area on the resulted images of (a) corrected scan images and (c) uncorrected scan images generated the quality of different line profiles of (b) the corrected scan images and the uncorrected scan images (d) using the proposed method (color online)

#### 4. Conclusions

It can be summarized from the observation results that the shift of the lateral images in x-axis was most probably caused by the scan-line shift. The causes of the shift may be due to uncertainty errors such as the effect of fringe scanning, installation, or motion error during the piezo-linear motor travel along the scan height.

The proposed method has been demonstrated and applied on two image datasets of scan-line shift during scanning by a modified Linnik Focale microscope. Although the measurement has a valid and accurate result in previous research, either the 3D image or the line profiler has distorted results. However, the scan-line shift is worth correcting with this proposed method, restoring the image alignment to the optimal position, and increasing the measurement accuracy of around 0.6 - 0.7% at the lateral axis quantitatively.

#### Acknowledgements

This research was supported by the IPP team at the ICube laboratory CNRS-Unistra France and the IPHC Laboratory.

#### References

- [1] A. Bosseboeuf, S. Petitgrand, *Microsystems Engineering: Metrology and Inspection III* **5145**, v1 (2003).
- [2] M. Guellil, P. C. Montgomery, P. Pfeiffer, B. Serio, *Optical micro and nanometrology V* **9132**, 913204 (2014).
- [3] P. C. Montgomery, M. Flury, F. Anstotz, S. Marbach, C. Cordier, J. Bartringer, H. Mukhtar, A. Leong-Hoï, A. Rubin, A. Shpiruk, M. Del Nero, and R. Barillon, *ACS Omega* **8**(12), 10643 (2023).
- [4] E. Halter, P. Montgomery, D. Montaner, R. Barillon, M. Del Nero, C. Galindo, S. Georg, *Applied Surface Science* **256**(21), 6144 (2010).
- [5] P. C. Montgomery, D. Montaner, F. Salzenstein, *Proc. SPIE* **8430**(2), 1 (2012).
- [6] H. Mukhtar, P. Montgomery, Gianto, K. Susanto, *IOP Conference Series: Earth and Environmental Science* **29**, 182 (2016).
- [7] P. J. de Groot, J. F. Biegen, *Optical Engineering* **55**(7), 074110 (2016).
- [8] A. Dubois, *Selected Topics in Optical Coherence Tomography*, ed. Gangjun Liu, INTECH, Rijeka, Croatia, 3 (2012).
- [9] L. O. O. Kittang, Norwegian University of Science and Technology, Department of Physics, Development and testing of a Linnik Interference Microscope for Sub-surface Inspection of Silicon during moving Indentation, 2012.

- [10] P. C. Montgomery, F. Salzenstein, D. Montaner, B. Serio, P. Pfeiffer, *Proc. SPIE*, **8788**, 87883G-1 (2013).
- [11] E. Pecheva, P. Montgomery, D. Montaner, L. Pramatarova, *Langmuir* **23**(7), 3912 (2007).
- [12] H. Mukhtar, P. Montgomery, F. Anstotz, R. Barillon, *Proc. SPIE* **10678**, 1067816 (2018).
- [13] G. Vizzeri, C. Bowd, F. A. Medeiros, R. N. Weinreb, L. M. Zangwill, *American Journal of Ophthalmology* **148**(2), 249 (2009).
- [14] G. Barteselli, D.-U. Bartsch, F. Viola, F. Mojana, M. Pellegrini, K. I. Hartmann, W. R. Freeman, *Bone* **23**(1), 1 (2014).
- [15] J. P. Kelly, F. M. Baran, J. O. Phillips, A. H. Weiss, *Translational Vision Science and Technology* **9**(10), 1 (2020).
- [16] P. Art, United States Patent, 19, 2000.
- [17] V. G. Badami, P. J. de Groot, *Handbook of Optical Dimensional Metrology*, 157 (2013).
- [18] I. Abdulhalim, *Journal of Modern Optics* **48**(2), 279 (2001).
- [19] I. Malinovsky, R. S. Franca, I. B. Couceiro, M. S. Lima, C. L. S. Azeredo, C. M. S. Almeida, J. P. Weid, 20th IMEKO World Congress **2**, 846 (2012).
- [20] A. Harasaki, J. C. Wyant, *Applied Optics* **39**(13), 2101 (2000).
- [21] P. C. Montgomery, D. Montaner, O. Manzardo, H.-P. Herzig, *Optical Micro and Nanometrology in Manufacturing Technology* **5458**, 34 (2004).
- [22] C. B. Lee, G. H. Kim, S. K. Lee, *International Journal of Precision Engineering and Manufacturing* **13**(9), 1509 (2012).
- [23] T. L. Schmitz, C. J. Evans, A. Davies, W. T. Estler, *CIRP Annals - Manufacturing Technology* **51**(1), 451002.
- [24] T. L. Schmitz, A. D. Davies, C. J. Evans, *Optical Manufacturing and Testing IV* **4451**, 432 (2001).
- [25] H. J. Von Martens, *Shock and Vibration* **4**(5-6), 327 (1997).
- [26] B. W. Guenther, P. J. Caber, P. E. A. Turner, A. E. D. Eisenberg, United States Patent 19, 1995.
- [27] I. Gaponenko, P. Tückmantel, B. Ziegler, G. Rapin, M. Chhikara, P. Paruch, *Scientific Reports* **7**(1), 1 (2017).
- [28] E. Bora, Master's Thesis, 2011.
- [29] W. Kaplonek, C. Lukianowicz, *Recent Interferometry Applications in Topography and Astronomy*, I. Padron (Ed.), Rijeka, Croatia, INTECH, 1 (2012).
- [30] J. Petzing, J. M. Coupland, R. K. Leach, *The measurement of rough surface topography using coherence scanning interferometry*, National Physical Laboratory, 2010.
- [31] I. Malinovski, I. B. Couceiro, M. S. Lima, R. S. Franca, J. P. von der Weid, *Journal of Physics: Conference Series* **575**(1), 012024 (2015).
- [32] S. Maraghechi, J. P. M. Hoefnagels, R. H. J. Peerlings, M. G. D. Geers, *Ultramicroscopy* **187**, 144 (2018).
- [33] F. Lagattu, F. Bridier, P. Villechaise, *Mater. Char.* **56**(1), 10 (2006).
- [34] M. A. Sutton, N. Li, D. C. Joy, A. P. Reynolds, *Exp. Mech.* **47**(6), 775 (2007).

---

\* Corresponding author: waczze@telkomuniversity.ac.id